# Structural Effects of Tempering on Cr Steels for Nuclear Fusion Reactors

L. BRUNELLI, P. GONDI and R. MONTANARI - Dipartimento di Ingegneria Meccanica - II Università di Roma - Tor Vergata

**Abstract**

*Structural evolution during tempering at various temperatures of martensitic steels has been followed by means of X-ray diffraction analysis, metallography in SEM and hardness measurements.*
*Effects of Cr content and of quenching rate have been considered. Persistence of large internal strains has been found even after full recovery of hardness. These strains are related with the large densities of bubble and void nucleation centres, which seem responsible for the swelling resistance of these alloys.*

**Riassunto**

Effetti strutturali della bonifica su acciai al cromo per reattori a fusione nucleare.
Si è seguita l'evoluzione strutturale di acciai martensitici durante riscaldamento a varie temperature mediante analisi di diffrazione dei raggi X, metallografia in SEM e misure di durezza. Sono stati presi in considerazione gli effetti del contenuto di cromo e della velocità di tempra.
Si è trovato che stati di tensione interna elevata permangono anche dopo un rinvenimento completo della durezza. Queste tensioni interne sono messe in relazione con le grandi densità dei centri di nucleazione di bolle e vuoti, che sembrano essere responsabili della buona resistenza allo swelling di queste leghe.

## Introduction

Martensitic alloys, submitted to suitable thermal treatments, seem promising for use as first wall materials in nuclear fusion reactors because of their swelling resistance, respect to austenitic alloys, which present swelling embrittlement. TEM observations of Wassilew et al. [1] and of Caciuffo et al. [2] have shown that, after high dose irradiation, bubbles form in martensitic alloys, in the grain interior and in the lath boundaries, with rather large densities and remaining small, in contrast to austenitic alloys, which show large increases of bubble dimensions [3].

With regard to physical origin of this behaviour specific of martensitic alloys several possible explanations have been proposed, based on the sink efficiencies of the dislocations [4] or on the presence of atypical loops [5]. Recently Odette [6] considers in this respect the effects of high sink densities with particular reference to the presence of large numbers of trapping sites at interfaces.

The present research deals at first with these interfaces, their characteristics and how they form; further, states of strain are considered, which may be responsible of large densities of trapping centres in the grain interior.

The observations have been carried out on 11% Cr and 9% Cr steels, in prevalence by X-ray analyses and SEM metallography. Preliminar results have been presented at ICFRM-3 [7].

## Experimental

The observations have been performed on martensitic steels with 11% and 9% Cr; the chemical analysis is given in Tab. I. All the specimens ($20 \times 30 \times 1$ mm$^3$) were preliminarly homogeneized for 30 minutes at 1075°C and then quenched with different cooling rates.

**TABLE 1 - Composition of the materials**

| Steels | Chemical composition (wt%) | | | | | | | | | | |
|---|---|---|---|---|---|---|---|---|---|---|---|
| | C | Cr | Mo | Ni | Mn | Nb | V | Si | Al | N | P |
| 11% Cr | 0.17 | 10.5 | 0.50 | 0.85 | 0.60 | 0.20 | 0.25 | 0.32 | 0.05 | 0.003 | 0.005 |
| 9% Cr | 0.12 | 9.0 | 0.92 | 0.35 | 0.45 | 0.08 | 0.22 | 0.35 | 0.04 | 0.050 | 0.015 |

The thermal treatments were carried out in Ar atmosphere and the temperature of the samples was continuously monitored during quenching. Temperature decrease between $T_h$ (homogeneization temperature) and $M_s$ (martensite start) was nearly linear; cooling rates $\dot{T}$ were determined using the expression $\dot{T} = (T_h - M_s)/\Delta t$ where $\Delta t$ is the cooling time between $T_h$ and $M_5$. The specimens, prepared in this way, underwent subsequent heat treatments of 1 h at 100, 200, 300, 400, 500, 600 and 700°C.

After each heating step, the specimens were cooled to room temperature and SEM observations, XRD analyses and microhardness tests were made always in the same zones. After polishing, 11% Cr steel was etched using Vilella reagent while 9% Cr steel was etched by means of a 10% HF + 5% $HNO_3$ + 85% $H_2O$ solution. The zones chosen for SEM observations were framed with microhardness imprints, used as reference marks. In this way it was possible to observe the microstructure evolution of the same areas after each heating step.

In order to attain informations about internal strains and grain dimensions, precision XRD line profiles were recorded and analysed by the Warren-Averbach method [8]. Grain orientation distributions were also determined by means of a Schulz camera. Vickers microhardness tests were performed with a load of 1 kg.

## Results

The structural effects of quenching rates, tempering treatments and Cr contents have been taken into examination.

For the 11% Cr steel and for two quenching rates, fig. 1a) shows the behaviour of the half height XRD line widths and of hardness for subsequent steps of heating at the temperatures indicated. The comparison with fig. 1b), referring to the 9% Cr steel, illustrates the effects of Cr content for the same treatments of tempering. Fig. 2 shows the behaviour of the half height widths for the 11% Cr steel, with a single temperature (700°C) of tempering in subsequent times for fast and slower quenching rates. It may be worth noticing that XRD spectra have not shown evidence of residual austenite. Metallographic aspects of the interest for the evolution of laths and of precipitation during tempering are illustrated in the SEM photos of fig.s 3. With reference to the texture observations, the stereographic projections of fig.s 4 are representative of the conditions before and after the heating treatment of tempering for the two Cr concentrations considered. To follow the texture evolution during the subsequent stages of heating, the densities in positions marked A, B and C on the azimuth circle of 40°, as indicated in fig. 4a), have been determined after each treatment. Fig. 5 shows the behaviour of the ratios between densities in B and A and in B and C.

Of the subsequent stages appearing in the structure evolution during tempering the first one starts from ~200°C and is more evident after rapid cooling from the austenitization temperature; it is characterized by:

— internal stress increases and/or subgrain size decreases as revealed by XRD line width increments;

— limited decreases of hardness;

— incipient disappearance of finer martensite laths;

— incipient reduction in the scattering of the grain orientations;

— appearance in SEM of specific dotted structures, with alignements consistent with the existence of subgrains within the laths, which act as sink for very small precipitates.

The second stage, from ~500°C, presents:

— a drop of hardness;

— concomitant internal stress decreases;

— lath disappearance and reduction of the grain orientation scattering, without drastic variations but appearing more as continuation of the processes begun in the first stage;

— evolution of precipitation with uniform distribution.

The effects of cooling rate together with those of Cr concentration are particularly strong on this stage.

The third stage, from ~700°C, is also more evident after rapid cooling rate and with the higher Cr concentration; together with the precipitate coarsening and the incipient recrystallization in evidence for this stage is considered the behaviour of internal stress, which decreases still remaining relevant.

## Discussion

Reference is made to the three stages on the basis of the various results.

The first stage is related to processes involving interstitial diffusion accompanied by local precipitation, probably of transition carbides, responsible for the dot alignements observed.

For sink at lath boundaries with distance l, the evolution from initial uniform concentration $C_0$ can be represented by the following equation:

$$C(x,t) = \frac{4}{\pi} C_0 \, e^{-\frac{\pi^2}{l^2} D \cdot t} \cdot \sin\left(\frac{\pi}{l} x\right) \qquad (1)$$

For the diffusion coefficient D of Carbon in α-Fe, concentrations $C(1/2,t) < C_0/10$ are obtained after t = 3600 sec. at 150°C for $l \simeq 4 \times 10^{-6}$ cm and at 200°C for $l \simeq 3 \times 10^{-5}$ cm. The lath dimensions observed in SEM correspond to the superior dimension. The XRD line width increases, evident at the onset of this stage for the faster cooling rates, seem not referable to internal stress increases since they are accompanied by constant or decreasing hardness; hence they are attributed to small subgrains forming within the laths in consequence of Carbon diffusion to sites of preferential sink. The XRD line profiles are consistent with subgrain dimensions of ~20 nm.

As consequence of dislocation unlocking and breakaway, migration of boundaries with lath disappearance may occur, if not hindered by precipitates forming in the boundaries themselves. This is confirmed by the observation in SEM of some lath disappearance, in particular of laths with smaller dimensions. The texture analyses show that lath disappearance reduces the scattering of crystalline orientations.

The first stage appears thus characterized by disappearance of smaller laths with unfavourable

orientations and development of fine subgrain structures, with precipitation of small carbides at subboundaries within the remaining laths.

For the second stage, its principal characteristic is the drop of hardness. After this recovery a fine scale subgrain structure was observed in TEM by Maziasz et al. [8] as well as by Caciuffo et al. [2] with negligible densities of free dislocations.

However, Fourier analysis of the XRD line profiles indicate that, together with that of subgrain dimensions, the contribution to line broadening of internal strains remains relevant.

The continuous line diagram in fig. 6 is the profile due to size contribution only, given by:

$$I(\vartheta) = C \cdot \frac{\sin^2\left[\frac{2\pi d\,(\vartheta_0 - \vartheta)\cos\vartheta}{\lambda}\right]}{\left[\frac{2\pi\,(\vartheta_0 - \vartheta)\cos\vartheta}{\lambda}\right]^2} \tag{2}$$

where C is a factor taken equal to $1/d^2$ for normalization, $\vartheta_0$ is the center of diffraction line and d corresponds to the dimensions obtained by the Warren-Averbach method; the experimental profile (dashed line), as obtained after correction by the Rachinger method, presents larger widths, especially in the lower part.

This phenomenon is particularly evident after fast cooling.

Given that full recovery of hardness occurs also after fast cooling, centres of internal strains, which do not cause hardening, have to be considered, probably depending on fluctuations of the Cr concentration connected with formation of α' phase [9].

Effects of precipitation of the metal carbides [10] are not considered as a possible cause of internal strain differences since precipitate coarsening appears independent of the quenching rates.

Finally, in the third stage recrystallization is accompanied by disappearance not only of the fine subgrain structure, but also by some decreases of the internal strains connected with inhomogeneities in the Cr concentration, at least for the slower cooling rates.

On account of the fine subgrain structure they observed, Maziasz et al. [11] have put forward the hypothesis that swelling is retarded in the martensitic alloys by the sink action exerted by the dense subboundaries, causing a large number of bubbles and voids to form. However this interpretation was criticized [6] since the subgrain structures of the martensitic alloys are similar to those presented by the austenitic alloys with lower swelling resistance. Our observations have indicated that, together with the fine subgrain structure, centres of strain are present, probably inhomogeneities of Cr distribution in ferrite, which may well act as sink centres. For the incubation exposures, the following expression has been given by Odette [6]:

$$\tau \simeq \frac{\Omega\, N_V}{m^* \dfrac{L_d}{(L_d + L_{sgb})}} \tag{3}$$

were Ω, $N_V$, $L_d$ and $L_{sgb}$ are respectively atomic value, void density, dislocation and subboundary sink strength; m* (the critical number of atoms per cavity) can be expressed in the case of an ideal gas as:

$$m^* \simeq \frac{4}{3}\pi\left(\frac{\gamma}{kT}\right)^3\left[\frac{\Omega}{\log\left(\dfrac{D_V \cdot C_V - D_I \cdot C_I}{D_{sd}}\right)}\right] \tag{4}$$

with $D_{sd}$-self diffusion coefficient, γ surface energy, $D_{V,I}$-vacancy/interstitial diffusivity, $C_{V,I}$-vacancy/interstitial concentration. According to expression [3], the increased swelling resistance may thus find an explanation in increases of $N_V$, depending on the fine structure of subgrains as well as on the inhomogeneities within subgrains, specific of the Cr distribution into ferrite. The observations of Gelles

et al. [12], who found increased swelling resistance with increasing Cr content, appear consistent with this explanation.

## Conclusions

The X-ray diffraction line analyses have shown the persistence of states of internal strain after treatments of tempering, which lead to full recovery of hardness in the examined Cr steel.

These states of internal strain decrease by decreasing Cr content and quenching rates.

Consistently with the various observations, these strains appear connected with characteristics of the Cr distribution, referable to the α' phase formation.

On account of bibliographical data on the effects of Cr content, these results appear consistent with the assumption that the increased swelling resistance of the martensitic alloys may also depend on these internal strains, which lead to increases of the void density proportional to the incubation exposure.

## References


[1] Wassilew, C., K. Herschbach, E. Materna-Morris and K. Ehrlich. Irradiation behaviour of 12% Cr martensitic steels. Proc. of *Topical Conference on ferritic alloys for use in Nuclear Energy Technologies*. (Snowbird) (1983), 607-614.

[2] Caciuffo, R., R. Coppola, F. Rustichelli and I.L.F. Ray. Investigation on He-bubble growth in α-implanted 1.4914 steel. *Journal of Nuclear Materials*, 155-157 (1988), 916-920.

[3] Maziasz, P.J. and C.J. McHargue. Microstructural evolution in annealed austenitic steels during neutron irradiation. *International Materials Reviews*, 32 (1987), 190-219.

[4] Sniegowski, J.J. and W.G. Wolfer. On the physical basis for the swelling resistance of ferritic steels. Proc. of *Topical Conference on Ferritic Alloys for use in Nuclear Energy Technologies*. (Snowbird) (1983), 579-586.

[5] Little, E.A., R. Bullough and H.M. Wood. On the swelling resistance of ferritic steel. *Proc. Roy. Soc. London*, A372 (1980), 565-579.

[6] Odette, G.R. On mechanisms controlling swelling in ferritic and martensitic alloys. *Journal of Nuclear Materials*, 155-157 (1988), 921-927.

[7] Coppola, R., P. Gondi, R. Montanari and F. Veniali. Structure evolution during heat treatments of 12% Cr martensitic steel for NET. *Journal of Nuclear Materials*, 155-157 (1988), 616-619.

[8] Warren, B.E. X-ray studies on deformed metals. *Prog. in metal physics*, 8 (1959), 147-202.

[9] Zhu, F., H. Wendt and P. Haasen. Atom probe field ion microscopy of Fe-Cr-Co permanent magnet alloy. *Scripta Metall.*, 16 (1982), 1175-1182.

[10] Elliott, C.K., G.E. Lucas, R. Maiti and G.R. Odette. Microstructures of HT-9 as a function of heat treatment. *Journal of Nuclear Materials*, 141-143 (1986), 439-443.

[11] Maziasz, P.J., R.L. Klueh and J.M. Vitek. Helium effects on void formation in 9Cr-1MoVNb and 12Cr-1MoVW irradiated in HFIR. *Journal of Nuclear Materials*, 141-143 (1986), 929-937.

[12] Gelles, D.S. *Fusion Reactor Materials Semiannual Progress Report*. DOE/ER - 0313/1 (1987), pp. 145.

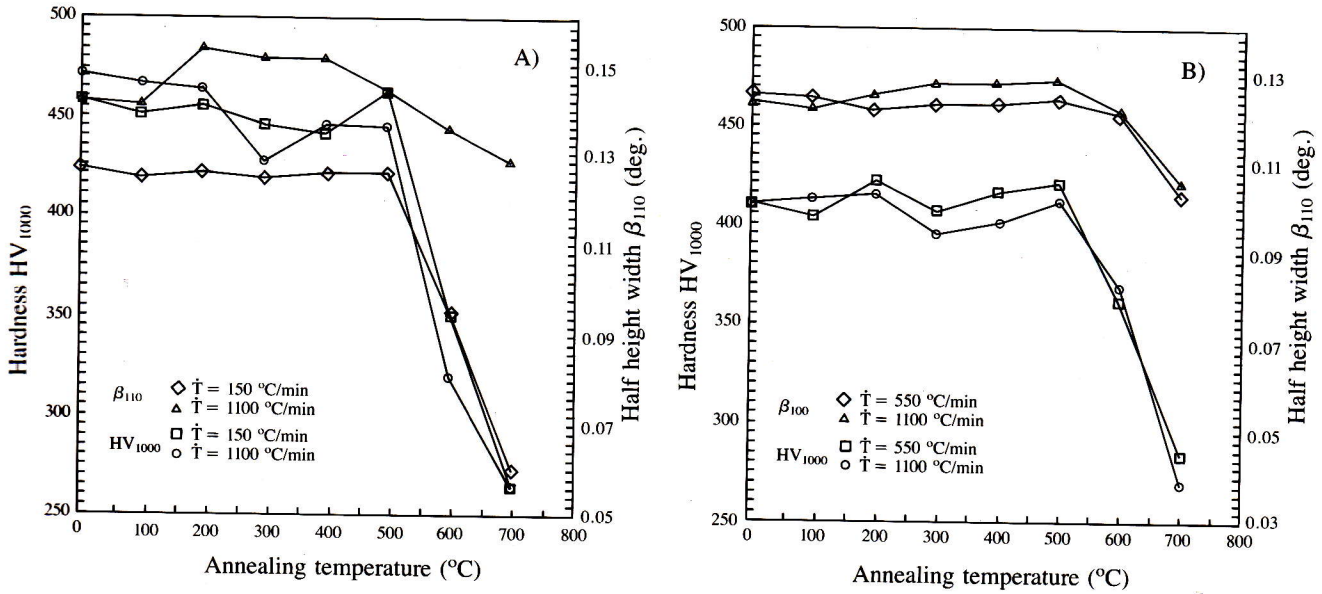


(a) steel 11% Cr

(b) steel 9% Cr

Fig. 1: Variations of XRD half height line width and of microhardness for subsequent thermal treatments of 1 hour at the temperatures indicated in abscissas. The figures show the comparison between specimens quenched with different cooling rates.

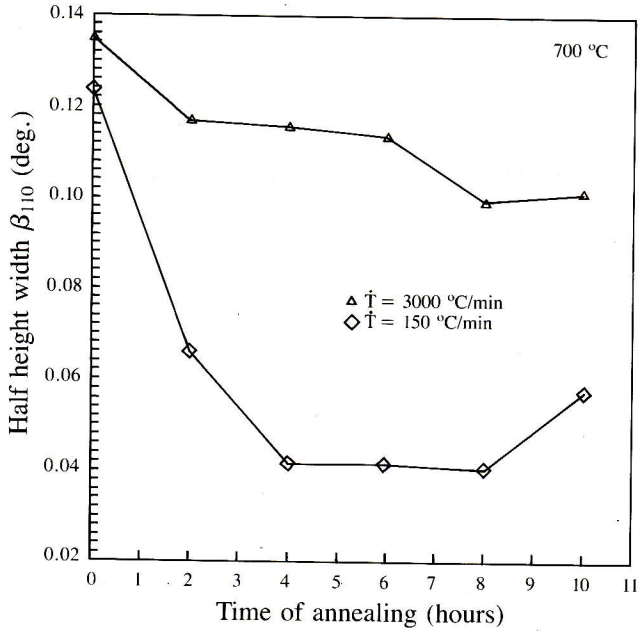


Fig. 2:
11% Cr steel: trends of XRD line width vs. annealing times at 700°C. Behaviour of specimens quenched with different cooling rates are compared.

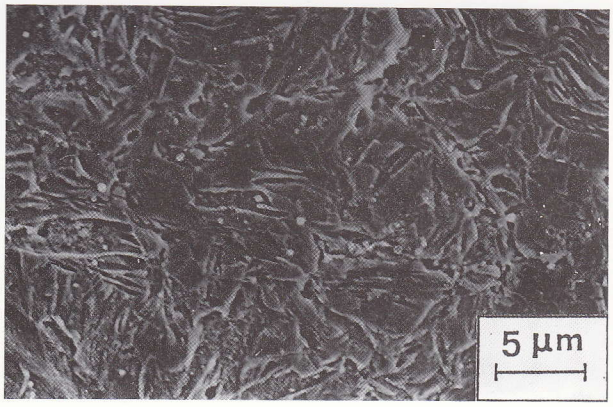


(a) as quenched

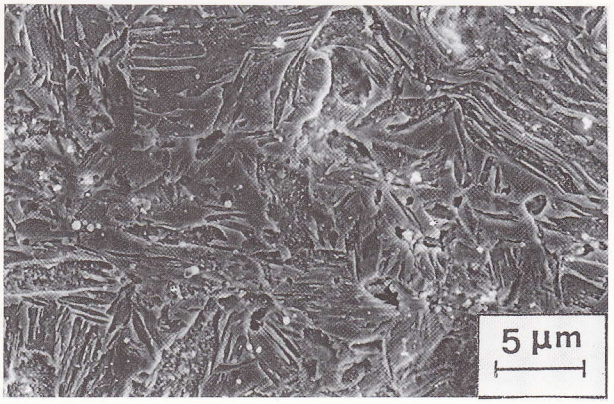


and after subsequent heet treatment of 1 hour at
(b) 100°C

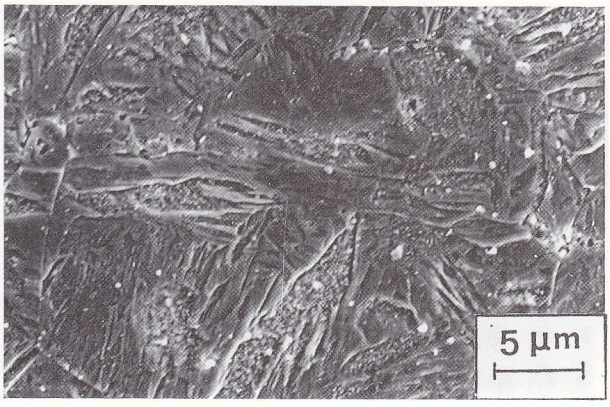


(c) 200°C

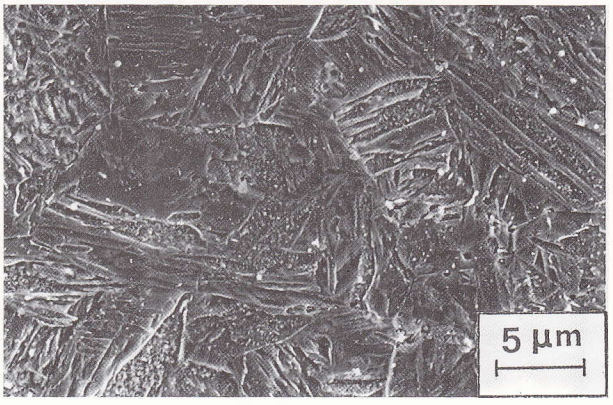


(d) 300°C

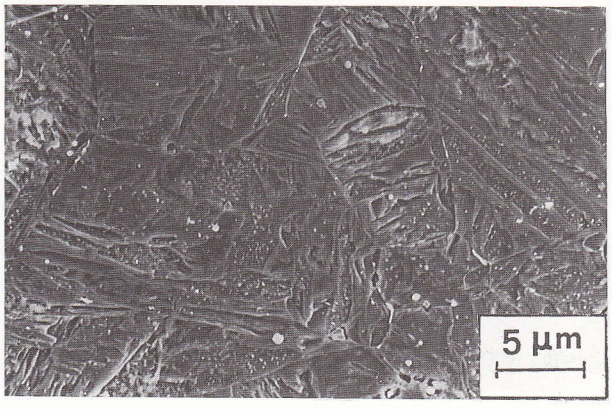


(e) 400°C


(f) 500°C

Fig. 3: SEM metallography of the same zone of a 11% Cr steel sample.

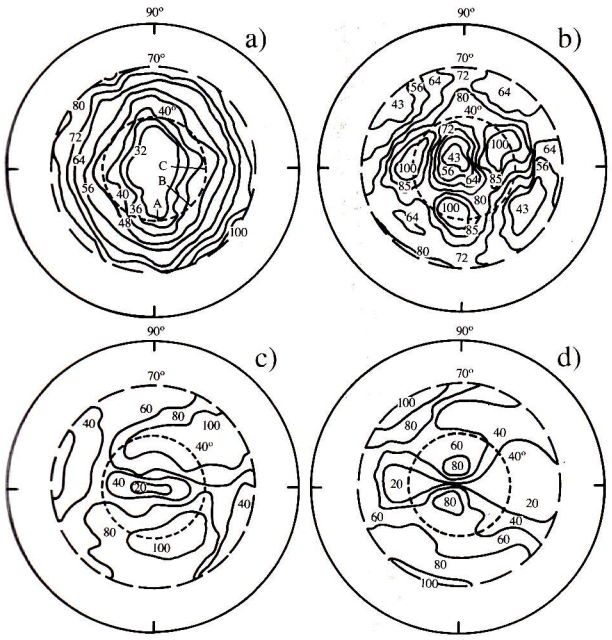


Fig. 4:
{110} Texture of 11% Cr steel (a – b) and of 9% Cr steel (c – d) in as quenched conditions (a – c) and after subsequent heat treatments of 1 hour up to 700°C (b – d).

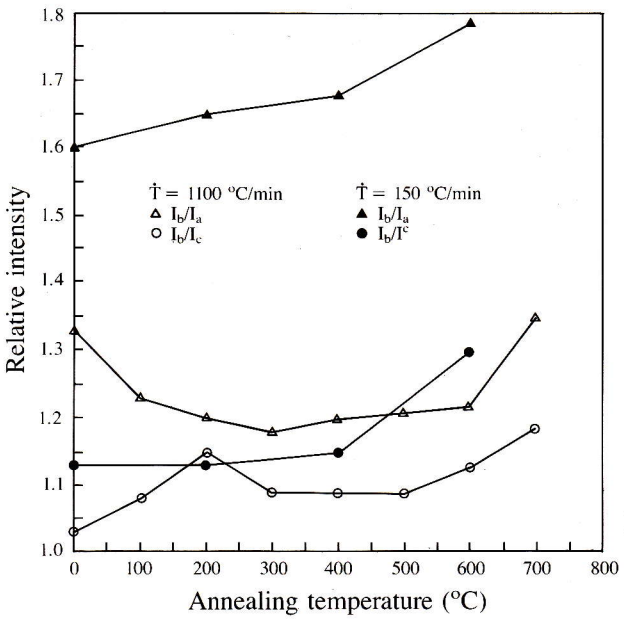


Fig. 5:
11% Cr steel: trends of $I_b/I_a$ and $I_b/I_c$ vs. annealing temperature. The parameters refer to {110} texture and to the grain densities (I) specific of the orientations indicated as A, B, C in fig. 4a).

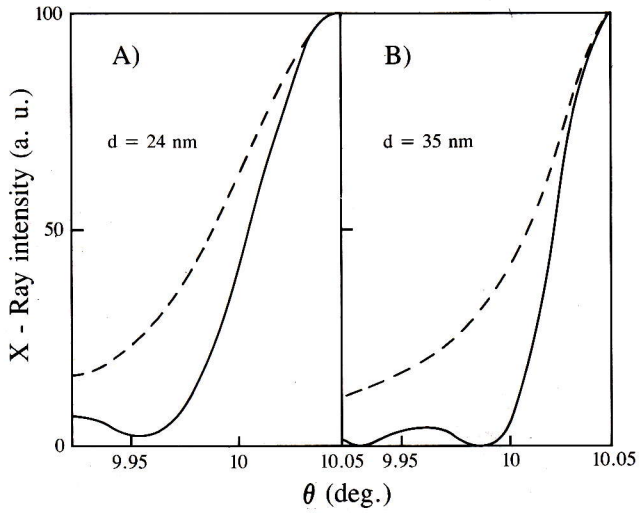


Fig. 6:
Experimental {110} XRD line profiles of 11% Cr steel specimens after quenching with rates $\dot{T} = 3300$°C/min a) and with $\dot{T} = 150$°C/min b) and then heated for 2 hours at 700°C. The continuous line represents the profile calculated using relation (2), i.e. the profile due to the size contribution only, for $<d>$ obtained from Warren-Averbach analysis.